Measuring the Pitch of CryoSat-2 Using the SAR Mode of the SIRAL Altimeter

Natalia Galin, *Member, IEEE*, Duncan J. Wingham, Robert Cullen, Richard Francis, Isobel Lawrence

***Abstract*—This paper describes the retrieval of the pitch of the CryoSat-2 satellite from full-bit-rate (FBR) SAR mode data collected over the ocean by the SIRAL altimeter. Starting with the FBR SAR mode data, we form beams at forward and backward look angles with respect to the nadir direction. If the satellite is flying pitched, the asymmetrical weighting of the echo power in the forward and backward-looking beams resulting from the along-track antenna gain pattern is used to measure the pitch of the satellite. The method depends on accurate knowledge of the orbit and the altimeter echoes only. In consequence, we are able to compare the results with the contemporaneous pitch value measured by the on-board star trackers, and, in particular, determine a bias in the star tracker pitch measurements. We find that the star trackers' pitch measurements are biased, with a constant offset of 0.055 ± 0.0073 degrees. Because the star tracker attitude is used to inform the on-board control system, this bias implies that CryoSat-2 is flying nose up with an average pitch of some 0.055 degrees.**

***Index Terms*—altimetry, calibration, CryoSat-2, mispointing, pitch, synthetic aperture radar.**

I. Introduction

CryoSat-2 is a European Space Agency satellite whose purpose is to measure fluctuations in the Earth's land and marine ice fields [1]. The satellite carries a single payload, a 13.6 GHz normal-incidence radar altimeter: "SIRAL". SIRAL has three modes of operation: 'low resolution mode' (LRM), 'synthetic aperture' (SAR) mode, and 'synthetic aperture interferometric' (SARIn) mode. The operating mode of SIRAL depends on the surface the satellite is overflying. In LRM, the satellite covers most of the world's oceans; it is acting as a conventional pulse-limited altimeter, such as ENVISAT [2], or Jason-1/2 [3]. In SAR/SARIn modes, the resolution is narrowed along-track by employing synthetic aperture techniques [4,5], and for SARIn a second antenna is mounted across-track to form an interferometer for across-track slope estimation [6]. The SAR/SARIn modes of CryoSat-2 have been specifically designed to improve data quality over the polar regions: SAR mode operates over sea ice, and SARIn mode over the continental ice sheets. The SAR/SARIn modes of SIRAL are the first of their kind in low Earth orbit. A detailed description of the CryoSat-2 mission, satellite, payload and operating modes is given in [1].

Altimeter missions such as TOPEX/POSEIDON, Jason-1/2 and ENVISAT all operate(d) in pulse-limited mode over the world's oceans for which analytical models [for example, 7,8] exist for predicting the shape of their pulse-limited echoes. These models are used operationally to extract measurements of the ocean surface height, swell wave height and wind speed. However, any error in the satellite pointing will affect the accuracy of these measurements, including those made in the pulse-limited, LRM mode of the SIRAL altimeter. The measurement errors vary quadratically with the 'mispointing' error, and although in detail they depend on the 're-tracking' algorithm, a pointing error of 0.1° will result in a height error of several cm [9].

Prior to CryoSat-2, the echo shape itself was the only data for routinely estimating the mispointing of a given satellite. [10,11]. CryoSat-2, however, is equipped with star-trackers (to allow the interferometric measurement of across track slope), which provide the attitude of the satellite in pitch, roll, and yaw. The star-trackers have an internal accuracy of a few arc-seconds. However, since the launch of CryoSat-2 in April, 2010, SARIn mode data collected over the world's oceans was used to calibrate the interferometer. This analysis revealed a static offset of 0.1065° (that is, a bias) between the roll angle reported by the star-trackers, and that measured by the interferometer [12]. It is understood that the error is in the rotation matrices applied to the star tracker quaternions to convert them to attitude angles with respect to the CryoSat-2 reference frame. Given the presence of a bias in the roll angle reported by the star trackers, it is likely that there is also a bias, perhaps of a similar magnitude, between the pitch reported by the star-trackers, and the pitch with which the satellite is actually flying.

In this paper, we describe a method for retrieving the pitch that the satellite is flying by analyzing the distribution of power in the synthetic beams observed over the ocean in SAR mode data, a method that is in some ways analogous to Doppler Centroid Estimation [13,14], now routinely used in SAR processing. In Section II, we describe the data used for this study. In Section III, we briefly describe the SAR algorithm used in CryoSat-2, and the resulting theoretical dependence of the star-tracker pitch on the pitch determined

Manuscript received October XX, 2013; revised October XX, 2013; accepted October XX, 2013. Date of publication October XX, 2013; date of current version October XX, 2013.

N.Galin is with the Laboratory for Satellite Altimetry, at the National Oceanic and Atmospheric Administration, College Park, MD 20740, United States (e-mail: natalia.galin@noaa.gov).

D.J.Wingham & I.Lawrence are with the Center for Polar Observation and Modelling, Department of Earth Sciences, University College London, WC1E 6BT London, U.K. (e-mail: djw@ucl.ac.uk; i.lawrence@ucl.ac.uk).

R.Cullen & R.Francis are with ESA/ESTEC, 1 Keplerlaan, Noordwijk, Netherlands (email: robert.cullen@esa.int; richard.francis@esa.int).

from the power in the synthetic beams. In Section IV, extraction of the pitch of the satellite from the power is described. It is compared with estimates of pitch from star tracker data and the bias between the star tracker data and the pitch of the satellite is calculated. In Section V, we make some concluding remarks related to our findings.

II. Satellite Configuration and Data

A full description of the CryoSat-2 satellite, its payload, the antenna bench assembly, and star trackers is provided and illustrated in [1]. In SAR mode, successive bursts (at 87.5 Hz) of 64 pulses with a PRF of 18.182 kHz are transmitted by one antenna, and the same antenna receives the reflected burst of 64 echoes. The received echoes are sampled, and 128 I, Q samples of each echo are stored and later downlinked from the satellite. These samples, converted to 8-bit numbers, together with orbit and attitude data, form the so-called 'full-bit-rate" (FBR) data. Its format is described in [14].

The SAR mode FBR data that we use were acquired over the South Pacific Ocean, drawn from a large region of SAR mode acquisitions in place from October 2012 [15]. We examined all the tracks that crossed this SAR mode latitude and longitude 'box' between 1st – 7th January, 2013, and chose a total of 26 tracks (Fig. 1) equally split between ascending and descending. We selected tracks long enough to allow allow us to retrieve 10,000 bursts falling within the box in the direction of travel, and whose pitch, as provided by the star trackers, was near zero. The pitch angles of these data are between 0.0050 to 0.0529 degrees.

The attitude of the satellite is provided by three star trackers mounted on the zenith side of the antenna bench close to the antennas. Each star tracker is oriented differently such that at any time at least one is free from sun- or moon-blinding. The star trackers provide the satellite orientation in an inertial reference frame by comparing the stars in their field-of-view with an on-board catalogue. The orientation is passed to the onboard navigation system, which, combining it with orbit information, converts it to a nadir-pointing reference frame, and informs the attitude control system of any adjustments that are needed.

The star tracker orientations are also used to calculate the antenna- and interferometer-baseline vectors, which are written to the data product, and accessible to the end-user.

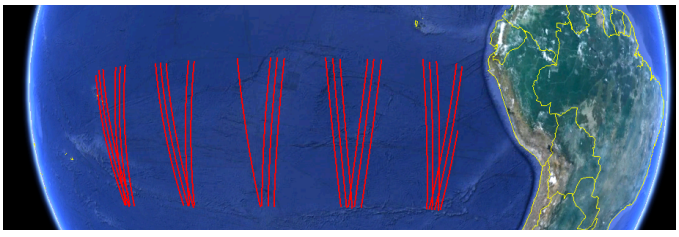

Fig. 1. The tracks of the 26 SAR mode FBR files used in the analysis.

These unit vectors are referenced to the CryoSat frame of reference in which x is in the direction of a unit vector pointing to nadir, y is parallel to a unit vector in the direction of the satellite velocity viewed from earth, and z is in the direction of a left-handed vector formed perpendicular to the plane containing the x and y vectors. The antenna boresight vector is nominally in the x-direction, the interferometer baseline vector nominally in the z-direction; in this study we use their actual components to approximate the attitude of the satellite as seen by the star-trackers; the pitch angle is to first-order given by the y-component of the antenna boresight vector , which is sufficiently accurate for our purpose. Using the sign convention set by ESA [16] a positive y-component of the beam direction vector, that is, a positive pitch, corresponds to CryoSat-2 flying nose down.

III. Relationship Between the Beam Power and Pitch

In SAR mode the echoes within a burst are phase coherent with respect to each other, and we are able using an FFT across the burst, the so-called 'azimuthal' FFT, to locate scatterers in the along-track direction. This process segments the real aperture of the antenna into a set of 'beams'. The bore-sight of each beam makes a different angle, or 'look-angle', with the nadir direction. A single beam is illustrated in Fig. 2; with the parameters of CryoSat-2, there are[1] 63 forward and aft beams around the nadir direction with a resolution of, and look angles separated by, 0.0238°. The theoretical distribution of echo power within each beam and between the beams (*i.e.,* across the burst) is described in detail in [1] and [17]. In summary, over a homogeneous rough surface such as the ocean, two aspects of the illuminating system determine the power distribution, within beams as a function of delay time, and also from beam to beam. The first of these is the change in illuminated area as a function of delay time of the pulses. For beams close to the nadir direction (see Fig. 11(a) of [1]) the illuminated area decreases rapidly with increasing delay time, hence the received echoes in those beams are of short duration and high amplitude; beams lying at appreciable look angles away from nadir have echoes of longer duration and lower amplitude. Of itself, this would result in a power distribution that is symmetric about the nadir direction, with a maximum in the nadir direction independent of the satellite pitch. But, secondly, the power between the beams is modulated by the along-track gain pattern of the antenna. If the antenna boresight is in the nadir direction, the power among the beams remains symmetrical. If, however, the satellite is flying pitched (as is shown in Fig. 2(b)) the antenna boresight is no longer in the nadir direction, and the modulation by the antenna pattern is displaced to an angle that is closer to the pitch of the satellite.

The effect of spreading in delay time of the off-nadir beams can be largely removed by integrating the power across delay time. The resulting power distribution, now a function of look direction only, is then predominantly that of the antenna pattern alone: its maximum lies at an angle that is very close

[1]The azimuthal FFT segments the real aperture of the antenna into 64 beams: 32 backward looking, and 31 forward looking (each illuminating approximately a 300 m strip on the surface). One of these, however, is the alias sample, which cannot be assigned a unique direction.

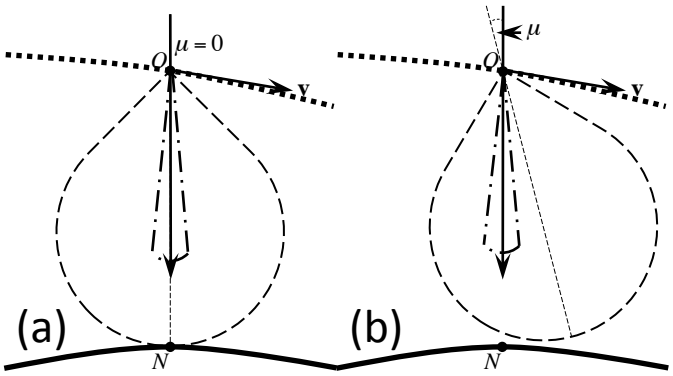

Fig. 2 illustrates the difference in illuminating geometry of a satellite flying at a zero and a non-zero pitch. The satellite is located at point '*O*', with its orbital path depicted by a dotted line, and the velocity vector extending as the tangent at *O* to the orbital path. A single nadir looking beam is drawn within the much wider along-track antenna gain pattern. Fig. 2(a) illustrates a scenario where the pitch of the satellite is zero; hence the power distribution between the beams either side of the nadir beam are symmetrically modulated by the antenna along-track gain pattern. If the satellite flies pitched, as shown in Fig. 2(b), the antenna gain pattern will have asymmetrically modulate the distribution of power across the beams. In general, the satellite velocity vector is not perpendicular to the nadir direction *ON*. This lack of orthogonality requires a phase correction to the azimuth FFT that is described in section IV.

to the pitch angle, and its distribution is close to the gain pattern of the antenna.

We have used the theory of [17], with the modifications suitable for the particular configuration of CryoSat-2 described in [12] to determine, with an accuracy well in excess of that needed for this letter, that the relation between the pitch μ, and the maximum of the beam power distribution μ_d, is a linear one, with a gradient that is close to, but slightly less than unity. If, in addition to the actual pitch, the star tracker measurement includes a bias μ_b, the relationship between the star tracker measurement μ_s and the maximum of the power distribution will be:

$$\begin{aligned} \mu_d &= 0.97\mu \\ &= 0.97(\mu_s - \mu_b). \end{aligned} \quad (1)$$

In this letter, we use a regression of the measured values of μ_s and μ_d to determine the value of the bias μ_b.

IV. Determination of the Satellite Pitch Angle

In this section, we describe how we retrieve the beam power distribution from the SAR mode FBR data and use it to measure the pitch of the satellite, μ_d. We then compare this pitch to the pitch from the star-trackers, μ_s, and obtain the value of the bias in pitch retrieved from the star trackers, μ_b.

Working with data of a burst we have 128 complex samples I+jQ from each of the 64 echoes per burst. First, we 'zero-pad' the 128 samples to 256 I/Q samples, and perform a 'range' FFT to form 64 complex echoes, each with 256 range, or delay-time, samples. We up-sample these complex echoes to avoid aliasing during the calculation of the power echoes.
Applying the azimuth FFT as described in [1] (see equations 2 and 3 of that paper) we then form the complex echo in each of the beams corresponding to the 63 look directions described above. We calculate the power echo falling within each beam from the modulus squared of the complex echo in that beam. Fig. 3(a) illustrates an along-track average of the power in the beams in each burst.

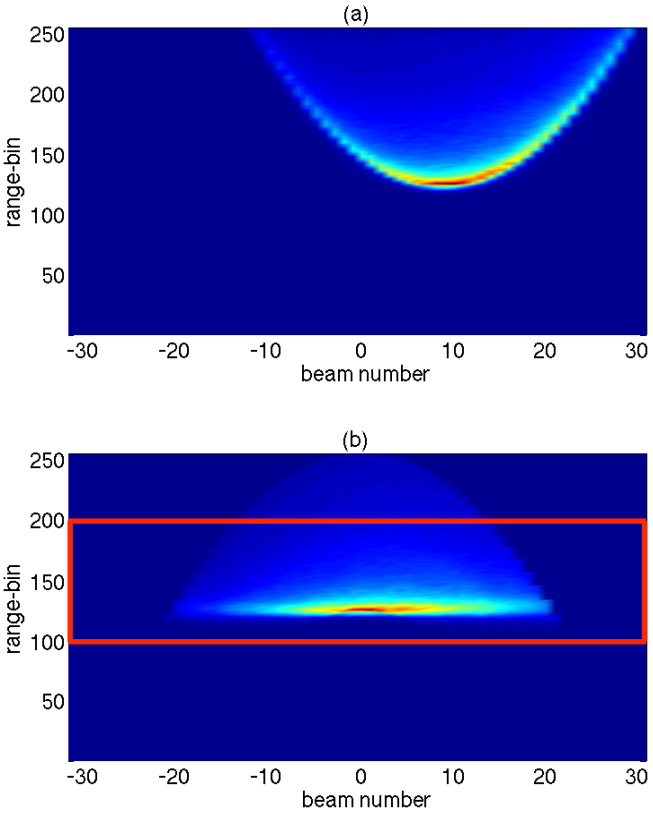

Fig. 3. The power distribution within and between the beams in an average of 1000 bursts of FBR SAR mode echoes. These data are taken from a SAR track on 1st January, 2013 (absolute orbit number: 14495). Fig. 3(a) shows the power distribution prior to slant range correction. The increasing range to the surface is clearly evident in beams at increasing look-angles. In Fig. 3(a) the 0th beam (DC component of the azimuth FFT) is orthogonal to the orbit vector, and the effect of the non-zero altitude rate is evident in the rightward shift of the beams. Fig. 3(b) shows the echoes after compensation for the altitude rate, and application of the slant range correction which aligns the receive time of the echoes within the beams to a common delay time. We expect that the distribution of power between the beams when we integrate the power (in delay time) within the red box will reflect the along-track antenna gain pattern.

The 0th beam is defined as the DC component of the FFT. However, because CryoSat-2 is flying in an elliptical orbit in which it experiences altitude rates as high as ±30 m/s near the equator, and the velocity vector does not generally lie orthogonal to the ellipsoidal normal at the nadir point. Fig. 2 illustrates a typical situation. The presence of a non-zero altitude rate will encode itself as a linear phase ramp across the synthetic aperture, with the result that an altitude rate shifts the 0th beam away from nadir. If this shift of the beams, which is apparent in Fig. 3(a), is not corrected for it may be interpreted as a satellite pitch. Using the altitude rate available in the FBR data, we calculate the effective phase ramp and correct for it. We also apply the slant range correction as described in [1]. The along-track average of the powers that result is illustrated in Fig. 3(b). (In the next step of the processing, described below, we integrate the data over the range dimension, and one can argue that then the slant-range

correction is unnecessary. This is true, but using it provides a check of the processing: if everything is correctly done, the echoes should all be aligned in range at this point, as is the case in Fig. 3(b).)

With the attitude rate corrected for, the 0^{th} beam now defines the beam directed in the nadir direction. Because we apply an azimuth FFT with a negative phase sign in its exponential, the echoes from scatterers ahead of the satellite will fall at positive beam numbers; those lying aft of the satellite will have negative numbers. In the example of Fig. 3(b), there is a residual asymmetry in the power with a maximum lying at positive beam numbers. This is a sign that the antenna bore-sight is pitched forwards of the nadir point, that is, the pitch is negative in the ESA data sign convention.

Each individual burst will suffer from a high degree of speckle noise, and hence, prior to examining the power distribution across the beams, we sum a total of 1,000 consecutive bursts, processed as described above. However, simple summation of the bursts is not possible as the on-board gating mechanism, which attempts to keep the returned echo at the center of the range-window, adjusts itself in 12.5ns intervals, leading to saw-tooth like shifts in the leading edge of the echoes. To avoid smearing of the echoes during summation along-track due to these tracking gate shifts, we align the starting point of the echoes first. We do this by averaging echoes of a burst prior to the azimuth FFT (each of these echoes is simply pulse-limited), then use the OCOG [18] retracker to calculate the epoch point of this mean pulse-limited echo, and finally interpolating the original complex echoes within each burst to align them to a common range-bin.

As described in section III, we look to the power distribution across the beams formed by the synthetic aperture processing of the echoes in a burst to measure the pitch. In theory, integrating the power of each beam effectively converts the instrument into a scatterometer, *i.e.*, a radar that measures the total energy that arrives from each illuminated area. That is, integrating the power of each beam over the entire range should largely result in the along-track antenna pattern. However, due to the slant-range geometry, the entire duration of the echoes in each beam is incompletely captured. We integrate the power in each beam across a fixed number of range bins, starting from range bin 100 (early enough to include any affects due to surface roughness) to range bin 200. The integration domain is illustrated by the red box in fig. 3(b). Fig. 4 illustrates a comparison between the result we obtain from an integration of the echo power in each beam with that we obtain from the theory of [12] that also includes these limits in its calculation. The theory treats the antenna pattern as a Gaussian, and it can be seen that the agreement is very close. These integration limits were also used in the theoretical calculation of the constant 0.97 in (1).

Fig. 3(b) shows that the range windowing is still present for beams either side of the maxima and these are excluded from the fit. As a result of the exclusion, the fit is calculated for beams between -15 to +20. The position on the horizontal axis of the Gaussian maxima is then μ_d, measured in units of beams width (0.0238°).

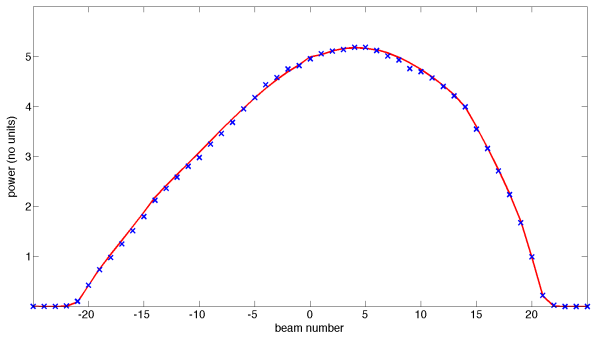

Fig. 4. The distribution of power across the beams from the data (blue dots) compared with the theory of [8] (red line) with a pitch of -0.1 degrees. The theory models the antenna pattern as a Gaussian: the extremely close match is a source of confidence that our method for pitch measurement is sound.

Fig. 5 shows a scatter plot of the pitch measured from the beam power distribution (μ_d) by applying the method to 10,000 consecutive bursts from the beginning of each of the 26 tracks shown in Fig. 1 (by averaging 1000 bursts we retrieve 10 data points from each file), compared with the star tracker pitch estimate (μ_s) from the contemporaneous values of the *y*-component of the beam vector in the FBR data. To remove outliers, data points lying more than three standard deviations from the regression line were removed. The subsequent linear fit to the remaining data (with 95% confidence intervals) is also plotted in Fig. 6, and is found to be:

$$\mu_d = \left[0.94 \pm 0.0111\right]\mu_s - \left[0.052 \pm 0.0003\right] \text{ degrees.} \quad (2)$$

From (2), we measure the bias in the star tracker data, that is, the value that the star trackers would report when the actual pitch of the satellite is zero, to be 0.0553 ± 0.0007 degrees.

The coefficient of 0.94 that we obtain is close to the theoretical value of 0.97 in (1), but is nonetheless significantly different. In order to be confident that the our results do not hide any effect on the pitch we retrieve from the echoes that depends on the roll of the satellite, or other parameters such as altitude, altitude rate, *etc*., we studied whether the residual error (*i.e.* the difference between the data and the line of Eq. 2) of each track had any statistically significant dependence on the roll, or any other orbit-related parameter. We found no such dependence. We suppose that there remains some subtle difference between the model we use and the hardware.

From the FBR data, we know that only star tracker '1' was used to generate the beam and baseline vectors in the data product. Strictly speaking, the result provides the bias of star tracker '1'. Fortuitously, we have access to SARIN mode L1b data the month of June, 2012, during which time there is data measured by all three star trackers. We have available to us the Vk1.0 version of the ESA SAR and SARIN L1 processor that allows us to select the star-tracker: by repeatedly running the processor, we were able to generate contemporaneous time-series of pitch from all three star-trackers. Our analysis of these values demonstrates that the average differences between their values are 0.0069 ± 0.0013 (between '1' and '2'), 0.0075 ± 0.0013 (between '2'and '3'), and 0.0024 ± 0.0014 (between '3' and '1') degrees.

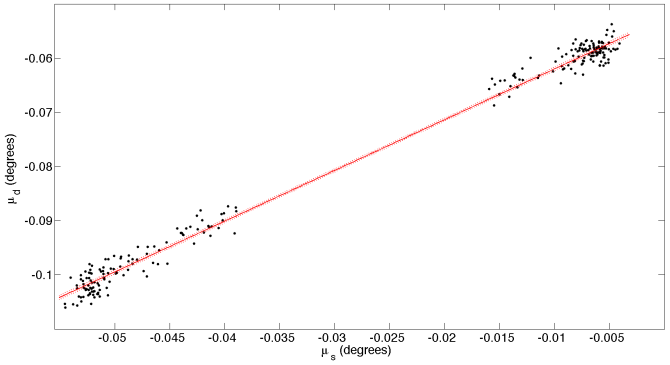

Fig. 5. The linear regression of the pitch measured from the beam power distribution versus that of the star tracker pitch. The linear regression is: $\mu_d = [0.94 \pm 0.111]\mu_s - [0.052 \pm 0.0003]$. The clustering of the data is an artifact of the orbit of CryoSat-2, that causes the pitch to vary depending on whether the track is ascending or descending.

The magnitude of these differences in pitch is much smaller than the measured bias, and they do not affect the value of the pitch bias. They are large enough to dominate the uncertainty of the bias. In conclusion, we measure the pitch bias in the star tracker pitch values, when using any of the three star trackers, to be 0.055 ± 0.0073 degrees.

V. Concluding Remarks

Our analysis has demonstrated a method for calculating the pitch of the satellite from the SAR mode FBR data. The measured pitch values tell us that the satellite is flying nose-up. We use our results to determine the bias in the pitch star tracker data. We show that in order to retrieve the actual pitch of the satellite from the *y*-component of the beam vector, whose sign convention accords a positive pitch to nose-down flight, an offset of 0.055 degrees should be subtracted from this value. A bias of this magnitude will result in cm level biases in the height precision, and its correction is needed for precise ocean altimetry with CryoSat-2.

The value reported for the pitch bias in this work differs significantly from another value of 0.0962 degrees reported in [19]. That value is based on fitting LRM echoes of CryoSat-2 to derive the square of the mispointing angle (ξ^2) and then exploiting the presence of the roll and pitch angles in the data product to determine which values of roll and pitch bias minimize in the least square sense the function:

$$f_{\min} : \xi^2 - \left[\left(\theta_s - \theta_b\right)^2 + \left(\mu_s - \mu_b\right)^2\right] \qquad (4)$$

where θ_s and θ_b are respectively the star tracker measured roll and roll bias.

Although it is not apparent to us why this way of working has resulted in different bias, we observe, firstly, that our method is uniquely sensitive to pitch so far as we have been able to determine. Furthermore, there is a discrepancy also in the roll bias of 0.0848 degrees reported in [19] and that of 0.1062 degrees deduced from a calibration of the CryoSat-2 interferometer (see [12]) whose accuracy is known to be 0.0015 degrees at 10 km scale lengths. As an additional check, we used our analysis to verify the along-track half-power beamwidth of the antenna. We obtained a half-power width of 1.0912 ±0.0077 degrees, compared with 1.09625 degrees determined from prelaunch measurements. This agreement to within 0.5% also gives us confidence in the bias we obtain.

Finally, the MATLAB code written to process the SAR mode FBR data, as well as the FBR data themselves used in these analyses are available on the website: [20].

References

[1] D. J. Wingham, C. R. Francis, S. Baker, C. Bouzinac, D. Brockley, R. Cullen, P. de Chateau-Thierry, S. W. Laxon, U. Mallow, C. Mavrocordatos, L. Phalippou, G. Raitier, L. Rey, F. Rostan, P. Viau, and D. W. Wallis, "CryoSat: A mission to determine the fluctuations in Earth's land and marine ice fields", *Adv. Space Res.,* vol. 37, no. 4, pp. 841-846, 2006.

[2] M. Roca, S. Laxon, and C. Zelli, "The ENVISAT RA-2 instrument design and tracking performance", *IEEE Trans. Geosci. Remote Sens.,* vol. 47, no. 10, pp. 3489-3506, Oct., 2009.

[3] Y. Ménard, L.-L. Fu, P. Escudier, F. Parisot, J. Perbos, P. Vincent, S. desai, B. Haines, and G. Kunstmann, "The Jason-1 mission", *Mar. Geod.,* vol. 26, no. 3/4, pp. 13-146, 2003.

[4] W. T. K. Johnson, "Magellan imaging radar mission to Venus", *Proc. IEEE*, vol. 79, no. 6, pp. 777-790, 1991.

[5] R.K. Raney, "The delay/Doppler radar altimeter", *IEEE Trans. Geosci. Remote Sens.*, 36, 1578-1588, 1998.

[6] Jensen, J.R., "Angle measurement with a phase monopulse radar altimeter", *IEEE Trans. Antennas. Propagation*, vol. 47, pp 715–724, 1999.

[7] G. S. Hayne, "Radar altimeter mean return waveforms from near-normal-incidence ocean surface scattering", *Antennas and Propagation, IEEE Transactions on*, vol. 28, no.5, pp.687-692, Sep. 1980.

[8] G. S. Brown, "The average impulse response of a rough surface and its applications", *Antennas and Propagation, IEEE Transactions on,* vol. 25, no. 1, pp. 67-74, Jan. 1977.

[9] E. Rodriguez & B. Chapman, "Extracting ocean surface information from altimeter returns: the deconvolution method", *J. Geophys. Res*., vol. 94, C7, pp 9761 – 9778, 1989.

[10] J.T. McGoogan, L.S. Miller, G.S. Brown, G.S. Hayne, "The S-193 radar altimeter experiment", *IEEE*, *Proceedings of*, vol.62,no.6,pp.793-803.

[11] L. Amarouche, P. Thibault, O.Z. Zanife, J.P. Dumont, P. Vincent, and N. Steunou, "Improving the Jason-1 Ground Retracking to Better Account for Attitude Effects", *Marine Geodesy*, vol. 27, no.1-2, pp. 171-197, 2004.

[12] N. Galin, D.J. Wingham, R. Cullen, M. Fornari, W.H.F. Smith, S. Abdalla, "Calibration of the CryoSat-2 Interferometer and Measurement of Across-Track Ocean Slope", *Geoscience and Remote Sensing, IEEE Transactions on.,* vol. 51, no.1, pp.57-72, Jan. 2013.

[13] I.G. Cumming, J.R.Bennett, "Digital Processing of Seasat SAR Data", *Acoustics, Speech, Sig. Proc., IEEE Conf.,* doi: 10.1109/ICASSP.1979.1170630

[14] CRYOSAT Ground Segment Instrument Processing Facility, L1b, Product Specification Format, CS-RS-ACS-GS-5106, [Online]. Available: https://earth.esa.int/documents/10174/125273/%5BPROD-FMT%5D_L1_Products_Format_Specification_v4.9.pdf/7bc7bdf6-3fef-4cc2-b7c9-b14437dcc6c2?version=1.0

[15] CryoSat-2 Geographical Mode Mask 3.4, [Online]. Available: https://earth.esa.int/web/guest/-/geographical-mode-mask-7107.

[16] CryoSat Product Handbook, [Online]. Available: http://emits.esa.int/emits-doc/ESRIN/7158/CryoSat-PHB-17apr2012.pdf

[17] D. J. Wingham, L. Phalippou, C. Mavrovordatos, and D. Wallis, "The mean echo and echo cross-product from a beam-forming, interfermetric altimeter and their application to elevation measurement", *IEEE Trans. Geosci. Remote Sens.,* vol.42, no. 10, pp.2305-2323, Oct. 2004.

[18] D. J. Wingham, C.G. Rapley, H. Griffiths, "New techniques in satellite altimeter retracking systems", *Proc. IGARSS'86 Symp.*, Zurich, 1986.

[19] W.H.F. Smith, R. Scharroo, "Retracking range, SWH, sigma-naught, and attitude in CryoSat conventional ocean data", *Ocean Surface Topography Science Team Meeting,* San Diego, 19-21 Oct. 2011.

[20] N. Galin, "MATLAB code for working with CryoSat-2 FBR data", [Online]. Available: https://github.com/ngalin/cryosat2_fbr2sar.